CHAPTER 7
DISRUPTION STUDIES IN JET

V. RICCARDO* *UKAEA/Euratom Association*
Culham Science Centre, Abingdon OX14 3DB, United Kingdom

Received May 1, 2007
Accepted for Publication October 5, 2007

Disruptions lead to the largest operational electromechanical loads on the vessel, its supports, and the in-vessel components. In addition, plasma-facing components can be exposed to very high thermal fluxes during the plasma thermal quench and to high-energy runaway electron beams. Therefore, disruptions represent one of the most demanding design load cases for this and the next generation of tokamaks, and they will need to be always strongly ameliorated or totally avoided in a commercial power plant. An overview of the observations and of the analytical and experimental work on disruptions carried out at JET both during the Joint Undertaking and under the European Fusion Development Agreement is presented.

KEYWORDS: *tokamak, plasma disruption*

Note: Some figures in this paper are in color only in the electronic version.

Contents—Chapter 7

I. INTRODUCTION

Plasma disruptions lead to a fast and irreversible loss of thermal and magnetic energy. The energy stored in the plasma is promptly released to the surrounding structures. Large toroidal loop voltages can accelerate runaway electrons, which may be lost to the vessel walls, causing metallic components to melt. Elongated plasma configurations can lose vertical stability[1]; if this occurs at full plasma current and thermal energy, it is called a vertical displacement event (VDE). When the plasma loses its equilibrium vertical position, it can contact the wall and part of its current (known as a halo current) can flow through the wall. A good understanding of disruption loads is important, since they have a strong influence on the operation of present experiments and on the design of any new tokamak device.[2]

The average poloidal halo current contributes to the vertical force on the vessel, while the local halo current density is a determinant in the mechanical design of in-vessel components. Currents induced in conductive in-vessel components both because of the plasma displacement and due to the plasma current decay also produce local and global forces. Electromechanical loads during disruptions at JET are reported in Sec. II.

The deposition of energy on plasma-facing components during disruptions can have a major impact on the lifetime of these components, and it is one of the main factors that have been taken into account for the determination of the divertor plasma-facing materials in ITER (Ref. 3). In Sec. III observations of predisruptive transients and disruption heat loads in JET are discussed.

*E-mail: valeria.riccardo@jet.uk

Long-lasting runaway electrons used to be generated at disruptions in JET before the divertor coils were installed in the vessel and the top/bottom symmetry was lost. Since the divertor installation, runaway electrons are still observed in fast current quench disruptions, but due to the increased vertical instability of the new, top/bottom asymmetric, machine configuration, they survive generally less than 100 ms. In addition, recently runaway electrons have systematically been produced in dedicated studies at low elongation and modeled using the self-consistent electron kinetics capabilities of the ARENA code[4] and other analysis tools. Section IV includes the discussion of the predivertor and postdivertor runaway electron observations and the recent numerical studies.

For us to learn to avoid disruptions or to predict them and to mitigate their effects, it is important to understand the physical mechanisms leading to them. Section V starts with the presentation of disruption classification and prediction neural networks developed for JET. In Sec. V also disruption mitigation by use of fast puffing of helium and higher-Z gases (neon and argon) is discussed. These techniques were applied to reduce poloidal halo currents only, due to limitations of the JET gas injection system at the time. In the near future a higher-pressure system will be ready for exploitation and its potential in reducing target heat loads and avoiding runaway electrons will be explored. In addition, as part of the disruption amelioration studies, neutral point (the plasma centroid position at which the initial plasma vertical displacement at the disruption is minimized) studies are presented.

II. ELECTROMECHANICAL FORCES DURING DISRUPTION

During disruptions the vessel, its supports, and the in-vessel components experience the largest electromechanical loads. These loads arise from the interaction of both induced currents and halo currents with the background magnetic field, in particular the toroidal field. JET disruptions can be divided into slow and fast:

1. Large plasma displacements at near-full current have high halo currents but are associated with slower current quenches.

2. Rapid current quenches induce high eddy currents but are accompanied by less halo current.

Therefore, these two sources of electromechanical loads can be at least partially decoupled and studied separately.[5]

II.A. Halo Current

A current flowing in the outer region of the plasma and having a part of its path in the vessel wall is called a halo current. While in the plasma, the halo current follows the magnetic field lines (under a force-free assumption); once in the conductive structures, it is free to choose the electrically easiest path between entry and exit points. The halo current is driven by the toroidal voltage induced by the core current decay and by the poloidal voltage due to the change in enclosed toroidal field, and it is also fed by the plasma motion convecting core current into the halo.

The technique employed in JET to estimate the poloidal halo current is to measure the variation of toroidal field within the halo current path outside the plasma. However, local current density and voltage drop measurements are also used. The history of the JET halo diagnostics is summarized in Table I and the location of each diagnostic is indicated in Fig. 1. A detailed description of the first generation of halo diagnostics (up to pulse 42 000) can be found in Ref. 6. A new set of halo

TABLE I

History of JET Halo Diagnostics

Diagnostic[a]	Type (Octant Number)	Pulse Range
A	Toroidal field pickup coil (3)	29 000 to now
A	Toroidal field pickup coil (7)	29 000 to 39 000
B	Toroidal field pickup coil (3)	29 000 to 43 000
C	Collected current at mushroom tiles (all 8)	29 000 to now (some failed)
D	Toroidal field pickup coil (4)	36 000 to 52 000
D	Toroidal field pickup coil (8)	44 000 to now
E	Poloidal shunts on divertor structure (1 and 5)	36 000 to ~50 000
F	Toroidal field pickup coil (1)	54 500 to now
G	Toroidal field pickup coils (3, 5, and 7)	54 500 to now
H	Rogowski coils (3, 5, and 7)	54 500 to now
Ii	Toroidal field pickup coils (1, 3, 5, and 7)	67 000 to now
Io	Toroidal field pickup coils (3)	67 000 to now
J	Rogowski coils (up to 8 in 1, 3, 5, and 7)	67 000 to now

[a]Also see Fig. 1.

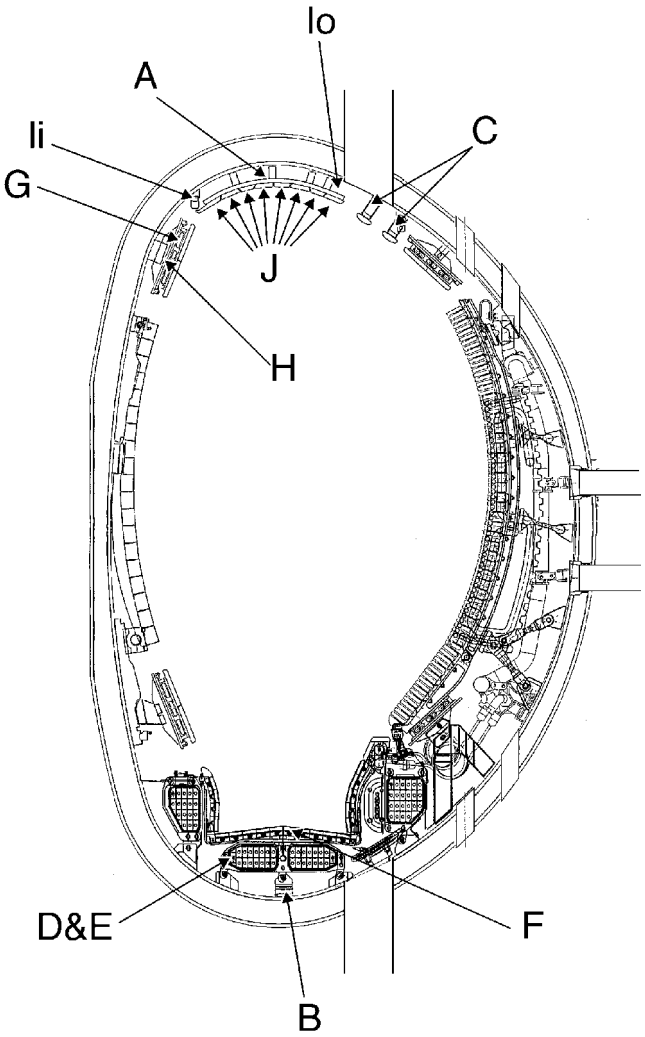

Fig. 1. Location of halo current diagnostics; the letter labels refer to Table I, where type, toroidal position, and pulse range of interest are detailed.

diagnostics was installed during the 2001 refurbishment (three toroidal field pickup coils and Rogowski coil assemblies located in the inner upper part of the vessel, behind the improved upper inner wall protections, or IUIWP), and the analysis of the data collected with these can be found in Refs. 7 and 8, respectively. The 2004 upgrade to the halo current diagnostic is described in Ref. 9.

The 2001 upgrade allows measurements of the poloidal halo current in a larger number of toroidal locations (three) than earlier in JET (two or fewer); if all four positions of the most recent diagnostic enhancement become operational, this will represent a further improvement. With the two original sets of probes at 180° (octants 3 and 7), the toroidal peaking factor (TPF; the ratio of maximum to toroidally averaged halo current) for a pure $n = 1$ mode could be underestimated by 50%, but with three probes at 90° (octants 3, 5, and 7), it can be underestimated by 25%, and with four probes (octants 1, 3, 5, and 7) at 90°, by only 15%. The TPF could be underestimated more if higher mode numbers were present. However, since the phase where the macroscopic plasma asymmetry ($m = 1$, $n = 1$) locks during disruptions is not fixed in JET (Ref. 10), the toroidal location of the highest poloidal halo current should have coincided with the toroidal location of one of the sensors over a large number of events. Figure 2 shows that the TPF measured by the IUIWP toroidal field pickup coils in recent disruptions ("2002+") is not larger than when it has been determined with only two probes ("1999−"). While the old discharges were selected from high-current events only, the new discharges are predominantly at low current. In addition, in comparison with the older discharges, the recent ones have similar elongation and generally higher triangularity. Therefore, the disruptions part of the recent data set had a stronger potential for more extreme halo currents; this explains the larger halo fraction observed in the new data. Figure 2 also contains the ITER reference design data for halo current.[11] The JET data are characterized by lower TPF values than most other machines. A possible explanation for this is that rather than direct halo current measurements, toroidal field measurements, which capture the current flowing in the vessel and are therefore intrinsically toroidally smoothed, are used.

Analysis of correlations between predisruption quantities and the severity of the halo current in the disruption that follows can help in identifying regions of the operational space prone to the highest electromechanical loads.

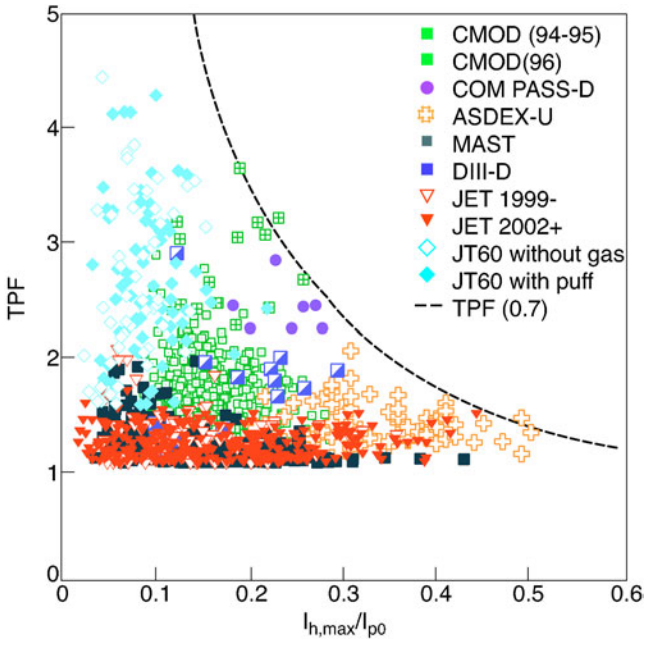

Fig. 2. Revised ITER halo current database.[11]

The halo current fraction correlates well with the vertical growth rate in JET. Since the vertical growth rate can be difficult to determine from the measured plasma vertical position due to the complexity of the event, an approximate formula is used in Ref. 8 for the vertical growth time τ_z (the inverse of the vertical growth rate γ_z):

$$\tau_z = \frac{1}{\gamma_z} = \tau_{shell}\left[\left[\frac{(1+k)^3}{(k-1)\left(\frac{d_{shell}}{a}\right)^2}\right]-1\right], \quad (1)$$

where

τ_{shell} = vacuum vessel penetration time for $m = 1$, $n = 0$ (5 ms for JET)

d_{shell} = characteristic torus dimension (sum of the minor semiaxes, 3.64 m for JET)

a = plasma minor radius

k = elongation.

In a number of controlled experiments, the simplified analytical approximation of the vertical growth rate has been found to be in good agreement with the measurements, especially for growth rates larger than 150 s^{-1}. From this experimental comparison, the error bars in Fig. 3 have been derived. The large horizontal spread is due to the variety of disruptive plasmas included in the database. The large vertical spread is due to a variety of disruption types included in the plot. VDEs give the largest halo fractions (for a given growth rate), and events with cold halo and core regions give the smallest halo fractions. Therefore, the largest halo fractions are to be found when high–growth rate plasmas lose vertical stability at near-full thermal energy (e.g., failure of the vertical control system, giant edge-localized mode, or low q). Moreover, Fig. 3 shows an upper limit to the halo fraction, which drops as the normalized vertical growth time increases. This is consistent with the observed proportionality between disruption vertical force measured at the vessel supports and initial plasma displacement vertical growth rate, since the poloidal halo current is one of the main contributors to the force applied to the JET vacuum vessel. The inverse dependence of the halo fraction on the normalized vertical growth time suggests that a closely fitting conductive shell, alternatively a passive conductor, is very important to be able to cope with highly shaped plasmas.

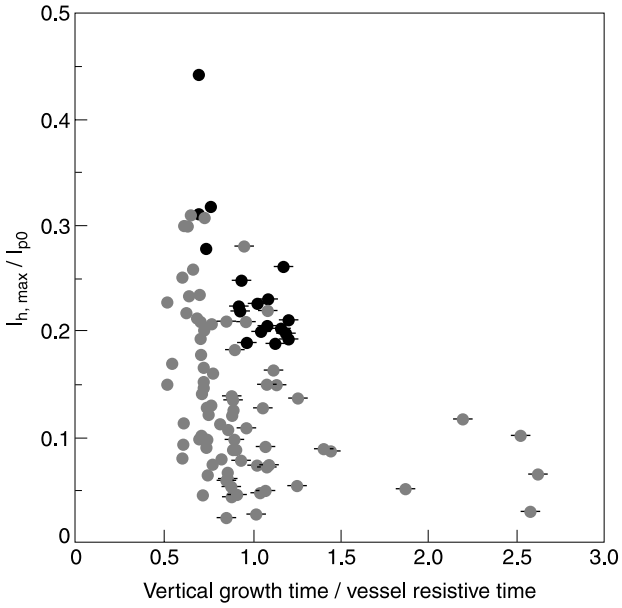

Fig. 3. The halo fraction plotted versus the normalized analytical vertical growth time (i.e., the ratio of the vertical growth time and the vessel resistive time), which is displayed with its estimated accuracy; the darker dots represent deliberate VDEs (Ref. 8).

II.B. Disruption-Induced Currents

The main source of induced currents during JET disruptions is the current quench itself, rather than the plasma displacement. This has been quantified in Ref. 12; therefore, only the current quench is addressed here. In Ref. 12 a database containing 791 events (pulse range 54 432 to 63 445) was analyzed. These events had plasma current between 1 and 4 MA (typically between 1.5 and 3 MA), toroidal field up to 4 T (typically between 1.5 and 3.5 T), and neutral beam power up to 22.5 MW. Very mild events have not been removed from the database.

Conventionally, for the ITER disruption database[2] (IDDB), the duration of 60% of the plasma current decay is used to estimate the quench rate. In JET the use of different intervals for the calculation of the linear plasma current decay rate highlights the limitations of each definition. Analysis of the distributions obtained using an interval that covers 100 to 40% or 80 to 20% of the predisruption plasma current shows that the mean is kept even though the spread is different. In delayed current decays (typically in VDEs, where the thermal quench occurs after a substantial plasma vertical displacement), the 100 to 40% linear approximation underestimates the quench rate. In current decays that slow down toward the end (e.g., due to the generation of runaway electrons), the 80 to 20% linear approximation underestimates the quench rate. Since in JET the disruptions providing the highest initial current decay rate are also those usually associated with the generation of runaway electrons, the use of the 100 to 40% definition for the linear decay rate results in the highest current quench rates.

The JET minimum current quench duration normalized to the predisruption plasma poloidal area, which is indicative of the plasma resistivity and hence of the post-thermal quench plasma temperature, is ~2 ms/m^2. This is similar to that from other tokamaks involved in the

IDDB (Ref. 2) and in more recent disruption studies.[11] Also, the normalized current quench duration derived from the instantaneous quench rate of JET (1.3 ms/m^2) is within the scatter of recent multimachine results[11] (1 to 2 ms/m^2). However, in many of the events with the highest instantaneous quench rate, the decay consists of several phases, so the peak current derivative can be used to determine inductive loads, but it is not physically related to the duration of the current quench.

The maximum of the linear current decay rate is ~200 MA/s, while the maximum of the instantaneous current quench rate is ~400 MA/s. In JET the ratio between the instantaneous and the linear decay current quench rates strongly depends on the type of disruption. The disruptions in which the ratio is largest are, apart from multiphase events, internal transport barrier (ITB) collapses, VDEs, and low-density locked modes. In most of the events in which this ratio is large, the current decay is fitted better by an exponential rather than a linear function, i.e., a constant toroidal resistance rather than a pseudoconstant loop voltage. The characteristic time for the fastest events varies between 7.1 and 9.6 ms and points to a postthermal quench electron temperature of ~3.5 eV, assuming $Z_{eff} = 2$.

The cumulative percentage of events as a function of the normalized linear decay current quench duration, plotted in Fig. 4, shows that 90% of the disruptions have a normalized duration longer than 3.3 ms/m^2 (in the 100 to 40% definition, and 3.9 ms/m^2 in the 80 to 20% definition). In addition, events between the minimum and 1.5 times the minimum duration represent a very small subset, about 5%.

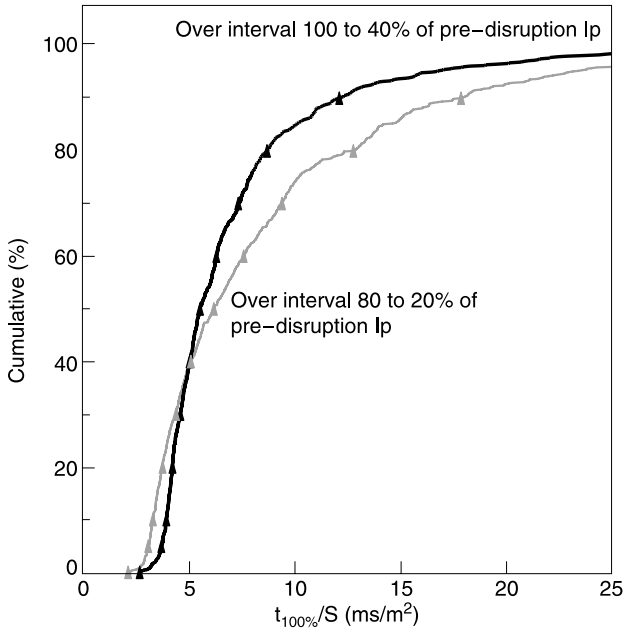

Fig. 4. Cumulative percentage of events as a function of increasing poloidal area–normalized current quench time[12] (e.g., 40% of the JET disruptions in the database have a poloidal area–normalized current quench time less than or equal to 5 ms/m^2).

II.C. Vertical Forces Acting on the Vacuum Vessel

Vertical forces are generated on the vacuum vessel as a result of the eddy and halo currents flowing in the vessel and in in-vessel structures following the loss of vertical stability during a disruption. These forces scale with the square of the plasma current as the contribution due to the change of toroidal currents (divertor coils and structure and other passive structures) and poloidal field generate vertical forces larger than those due to poloidal halo currents crossing the toroidal field. The value of the vertical force depends on the plasma configuration and the type of disruption as well. In JET a so-called F number has been used[13,14] since the late 1980s as an empirical estimate of the maximum vertical force that can be generated by a given configuration, and it has been routinely calibrated against the forces measured in disruptive discharges. For a given configuration and at comparable plasma current, the disruptions that produce the largest vertical forces are those caused by VDEs, where the loss of vertical stabilization generates the largest variation in vertical current moment. On the other hand, disruptions in which the control of the vertical position is maintained during the decay of the plasma current produce small or negligible vertical forces.

II.D. Sideways Displacements

Asymmetric VDEs are fortunately rare in JET. They can produce large net lateral forces and vessel displacements (observed up to 7 mm in a 3.5-MA, 2.8-T pulse), which have caused significant mechanical damage to components attached to the vessel, e.g., to the neutral beam box rotary valve in 1995 (pulse 34 078). Since the 1996 shutdown a toroidal belt has been added to the outer midplane to limit the extent of the vessel displacement.

A simple model[15] based on the asymmetries in the vertical current moment allows the lateral forces generated during asymmetric events to be estimated as a function of plasma current and position measured in four octants (1, 3, 5, and 7). This model, coupled with a lumped-parameter mechanical model of the vessel and its supports,[16–18] has been validated by predicting the displacement history of the JET tokamak caused by a number of major asymmetric VDEs. Figure 5 shows the vessel support lumped-parameter model; the inset shows a comparison between the direction of movement predicted by the analytical model and measurements for some of the events with the largest vessel sideways displacements. A more rigorous analysis for the force acting on the vessel during asymmetric VDEs (Ref. 19)

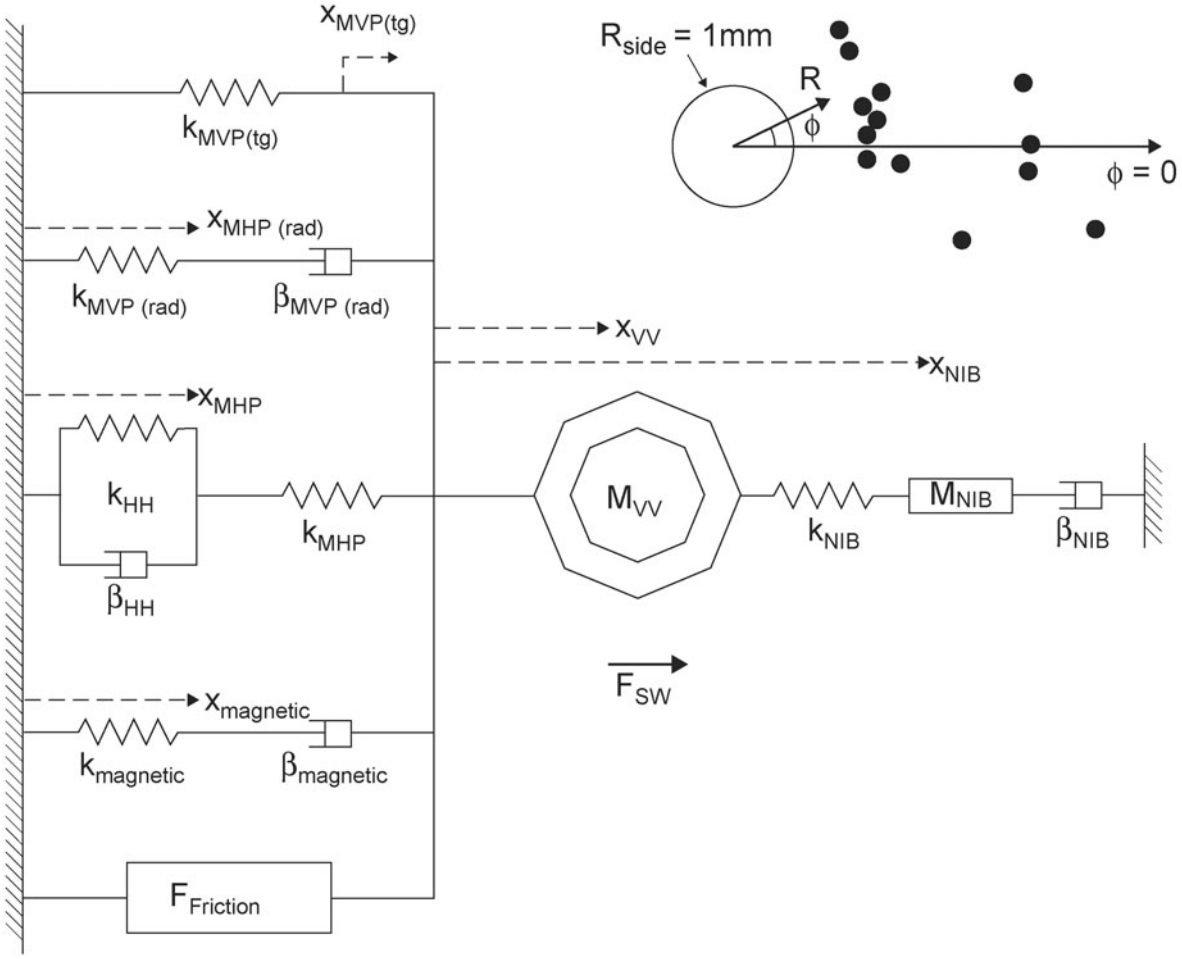

Fig. 5. The lumped-parameter model of the JET vacuum vessel[15] is a set of equations capable of predicting the sideways displacement history as a function of an applied lateral magnetic force. The vessel constraints are the main vertical ports (MVP), the main horizontal ports (MHP) and their hydraulic horizontal (HH) belt, the magnetic force the vessel itself creates while moving in the external toroidal field (magnetic), and the neutral injection boxes (NIB). The inset shows a comparison between the analytical model and measurement. Once the predicted direction of the impulse has been computed, the coordinates have been rotated so that the computed sideways impulse vector points toward $\phi = 0$ and the measured sideways displacements are plotted in this rotated coordinate system, confirming that the direction of the impulse was predicted by the model.

reveals that the repelling force between the plasma and the vessel is of little significance in asymmetric events, even if it is the main symmetric repelling force. The sideways force acting on the vessel is shown to be due mainly to the interaction of the asymmetric circulation of currents in the wall with the toroidal field. The source/sink of the asymmetric wall current is given by the imbalance between the influx and the outflow of perpendicular (poloidal) halo currents at any toroidal location. For an $m = 1$, $n = 1$ macroscopic asymmetry, the current variation as a function of toroidal angle is expressed by $\delta I_p \cos\phi$. The continuity equation gives the current per unit length flowing vertically from the plasma into the top part of the vessel as $j_v(\phi) = \delta I_p / R \sin\phi$. The wall has zero divergence, apart from a thin ring where the current enters/exits. Therefore, the vessel current density can be expressed in terms of a stream function and the toroidal and poloidal components of the wall current estimated as

$$j_\phi = -\frac{\delta I_p}{p}\cos\phi$$

and

$$j_s = \frac{\delta I_p}{2R}\,\frac{p-2s}{p}\sin\phi \ ,$$

where p is the poloidal perimeter of the vessel and s a poloidal coordinate (varying between 0 and p). Integration

over the vessel of the vertical projection of the poloidal vessel current path gives a net sideways force $\sim \pi B_{tor} b \delta I_p$, where b is the vertical semi-axis of the torus.

III. ENERGY DEPOSITION DURING DISRUPTIONS

Power losses to the plasma facing components during disruption are observed using infrared systems and, in the divertor, thermocouples. The divertor is observed by an infrared camera, which detects photons in the 3- to 5-μm wavelength region.[20] The detector collects data on four two-dimensional subarrays (64×64 pixels each) at a rate of $\sim$20 μs per line. The field of view is split into two tangential views of the inner and outer divertor so that both strike points are visible for most plasma configurations. Embedded in the JET divertor target tiles are more than 40 thermocouples.[21] These are fitted 10 mm below the plasma-facing surface and are evenly distributed poloidally. The thermocouples provide a reasonable poloidal profile of the disruption energy distribution on the divertor. While only discrete toroidal locations are viewed by the infrared cameras, the thermocouples are distributed over several of the 24 divertor modules and show that typically disruption heat loads are evenly distributed.[22]

The total energy radiated during the disruption can be estimated using the JET bolometry. The thermal energy at the quench is estimated from measurements of the plasma temperature by electron cyclotron emission[23] (ECE) and the chord-integrated soft X-ray (SXR) emission from the plasma.[24] Both measurements are routinely available with high time resolution (better than milliseconds) in JET and thus allow determination of the temporal characteristics of the thermal quench processes. These cannot be studied in JET in the usual way (i.e., by diamagnetic methods) due to the fast magnetic field changes that occur during this phase.[25]

III.A. Energy Deposition During Predisruptive Loss of Plasma Performance

The analysis of the plasma thermal energy once the plasma performance has already degraded before disruption conditions are reached, often several confinement times before, has been carried out on a database including 129 disruptions of plasmas reaching at least 4.5 MJ of thermal energy at any point in the discharge (over the pulse range 54 432 to 63 445). The energy threshold of 4.5 MJ has been chosen to select a group of "high-energy" discharges that have the potential to exceed 1.5 MJ/m^2 divertor energy density at the thermal quench. The detailed procedure to estimate this energy density is presented in Ref. 26. An energy density of $\sim$1.5 MJ/m^2 in timescales of 0.2 to 3.0 ms is sufficient to cause significant material damage.[27] In fact, the "ablation/melting parameter"[28] ϕ_{damage}, which determines the expected surface temperature rise caused by the transient energy pulse, can reach values up to 28 to 106 MJ m^{-2} s$^{-1/2}$. This is in the range of values resulting in significant carbon evaporation and tungsten melting[28] ($\sim$40 to 50 MJ m^{-2} s$^{-1/2}$); note that there are no tungsten plasma-facing surfaces in JET to date.

For most disruptions the energy loss can be divided into two phases:

1. slow loss (thermal collapse) of thermal energy prior to the onset of the disruption, on time scales of the order of the energy confinement time
2. fast loss (thermal quench) of thermal energy at the onset of the disruption (e.g., due to fast-growing magnetohydrodynamics), on time scales of milliseconds (or submilliseconds)

Of the 129 "high-energy" disruptions in the database, only 20 reach the maximum thermal energy less than 1 s before the disruption. The vast majority, $\sim$80%, of the discharges reach the disruption thermal quench with less than 50% of thermal energy at full performance, and 65% maintain less than 30%. Indeed, the loss of plasma performance is often used to soft-land discharges in order to either limit the machine activation or prevent possible disruptions. Although the intermediate to high range (60 to 90%) of predisruptive energy normalized to full performance energy is only sparsely populated, the high end of the spectrum has a local large relative probability (12%). This spike in the tail of the distribution is mainly comprised of disruptions occurring in ITB discharges with strong transport barriers. The shape of this distribution does not change when JET-specific disruption amelioration actions (e.g., power removal under real-time control, or basic reduction of plasma elongation to limit disruption forces) are removed. This is achieved by dividing the energy left at the thermal quench by the thermal energy the plasma would have had according to the ITER-98(y,2) scaling law rather than to the thermal energy it had when at full performance. Figure 6 shows the distribution of "high-energy" disruptions with respect to the thermal quench energy normalized to ITER-98(y,2) thermal energy. With this normalization the average plasma energy at the thermal quench in JET is $\sim$40% of the one that the plasma would have if it kept the high-energy confinement H-mode confinement at this stage. These observations, together with similar ones in ASDEX Upgrade,[29] have motivated the reevaluation of the ITER disruption design criteria for ELMy H-mode operation.

III.B. Thermal Quench Parameters

The duration of the thermal quench in JET is estimated by analyzing the time evolution of the ECE electron temperature measurements in the central region of the plasma. The channels selected for this analysis

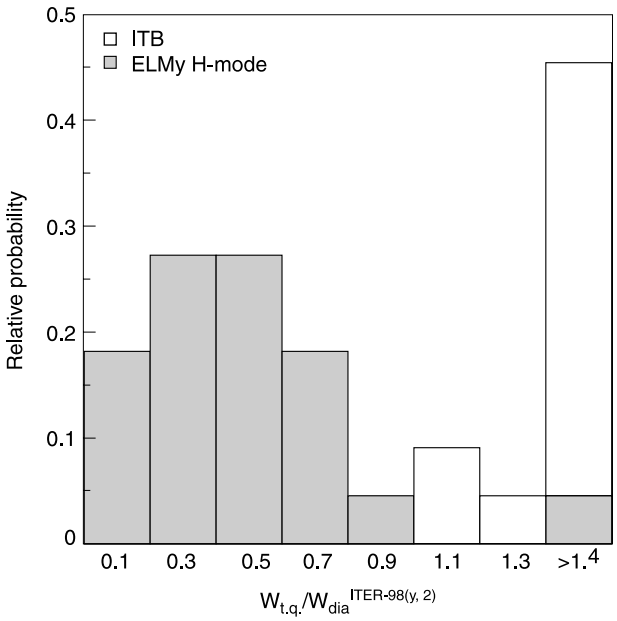

Fig. 6. Relative probability for the fraction of disruption thermal energy, taken as the ratio between the measured thermal energy just before the thermal quench and the estimated ($H_{98(y,2)} = 1$) thermal energy at this time for a set of "high-energy" JET disruptions.[26]

provide the temperature during the thermal quench as close as possible to the magnetic axis of the discharge, while avoiding channels in which the measurement is invalidated by the presence of suprathermal electrons or ECE emission cutoff.

The collapse of the electron temperature in most disruption types occurs in two phases in which an initial large flattening of the temperature profile is followed by a constant-shape decrease of the flattened profile. The size of the temperature decrease in the two steps and the time scales for these two phases vary from disruption to disruption; sometimes the two phases merge into one. Due to the variability of the central temperature evolution during the thermal quench, two ways of characterizing the duration of the thermal quench are used:

1. a global thermal quench timescale given by linear extrapolation of the time required for the central electron temperature to drop from 90 to 20% of its predisruptive value. This definition is applied independently of the number and duration of previous downward steps, provided that a significantly large final downward step in the temperature can be identified (typically a few hundred electron volts).
2. a timescale for the last step in the temperature collapse during the thermal quench. This is again on the drop between 90 and 20%, but it is applied when a clear redistribution phase can be identified.

Figure 7 compiles the results of the analysis of a subset of the 129 "high-energy" disruptions. In Fig. 7a the duration of the thermal quench extracted using the two definitions above is plotted versus the plasma thermal energy from the closest reliable diamagnetic energy measurement to the thermal quench time. Both the "global," or single-step, values and those of the second step, when it can be determined, are plotted in Fig. 7a for discharges in which ECE measurements are available with standard time resolution (~300 to 400 μs). The data in Fig. 7a demonstrate that the typical timescale for the flux of plasma thermal energy from the bulk plasma into the edge plasma during disruptions in JET is in the range of 0.2 to 3.0 ms. The shortest times are routinely associated with ITB disruptions due to an excessive pressure peaking. The variability of the duration of the thermal quench in JET disruptions is large, and no correlation between the measured timescales and the plasma parameters at the thermal quench could be identified in the existing database.

When considering very fast thermal quench collapses, the typical timescale of the thermal quench becomes comparable to the time resolution of the ECE measurements with standard data acquisition speed (~300 to 400 μs). To determine the duration of these fast thermal quenches, the use of faster ECE measurements is necessary. These measurements exist for a very restricted number of discharges. The comparison between the thermal quench timescale as determined by the "global," or single-step, duration with the standard (300- to 400-μs) and the fast (4-μs) ECE measurements is shown in Fig. 7b, which shows that the standard time resolution for the ECE data is sufficient to characterize the thermal quench timescale of most disruption types (with a maximum error of 30 to 40%) with the exception of high-pressure peaking ITB disruptions. These ITB disruptions have typical timescales of ~100 μs and therefore require ECE measurements with the highest temporal resolution (4 μs) to be resolved. Figure 8 shows that although the minimum duration of the thermal quench measured with the slow time resolution ECE (~400 μs) matches the "old" JET data supplied to the IDDB in Ref. 2 (Fig. 54), the one estimated using the ECE fast resolution (~50 μs) falls significantly below. The reduction in the duration of the observed thermal quench is due not only to the improved diagnostic sampling rate but also to the inclusion in the analysis of more disruption types, in particular ITBs. The timescale provided by the ECE analysis is not that of the timescale for the flux of energy onto plasma-facing components (PFCs) during the thermal quench but that of the energy loss from the bulk plasma during this phase. However, this does provide a minimum value for the duration of the phase over which energy is deposited onto PFCs.

Quantitative measurements of the PFC temperature rise time at the disruption and of the power deposition footprint are not available in JET due to limitations of the

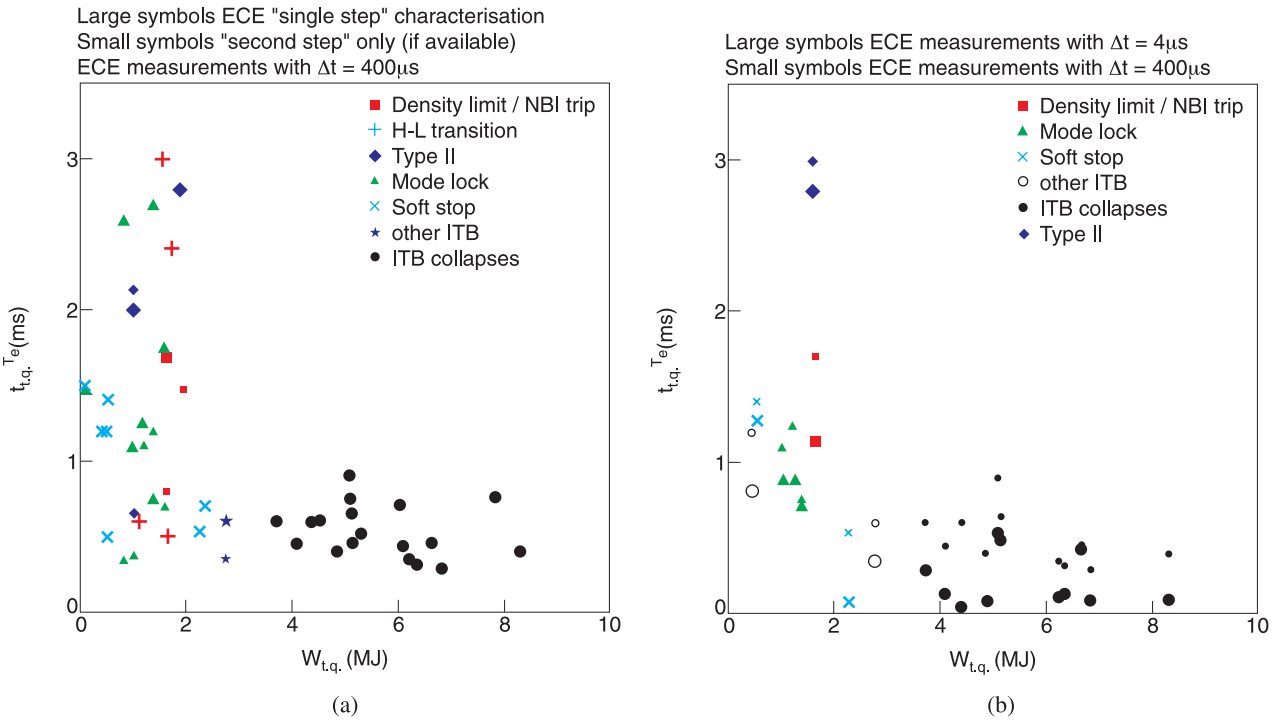

Fig. 7. Duration of the thermal quench versus the predisruptive plasma energy. (a) Standard data acquisition ECE measurements: single-step process (large symbols) and second step (small symbols, for discharges in which the temperature profile redistribution is observable with standard data acquisition). (b) Single-step process for discharges in which both the standard (small symbols) and the fast (large symbols) acquisition ECE measurements are available.[26]

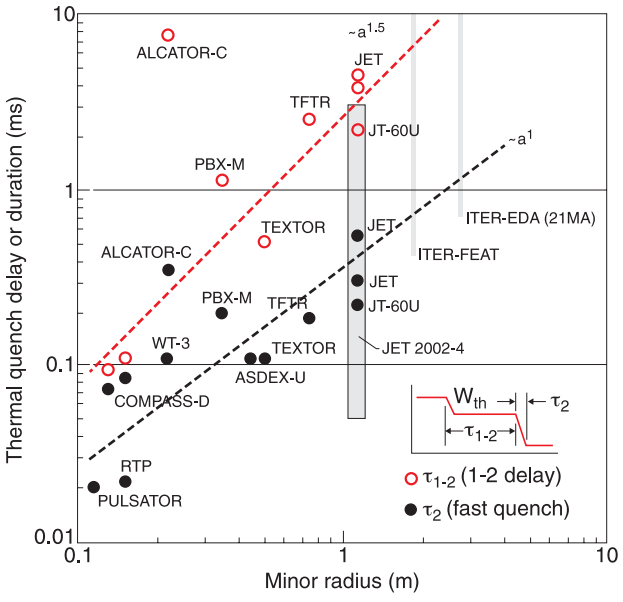

Fig. 8. ITER Physics Basis (Ref. 2, Fig. 54) thermal quench times overlapped with the thermal quench duration measured in some recent "high-energy" JET disruptions[26] (labeled JET 2002-4).

diagnostic systems. Energy balance cannot be achieved if only the energy collected in the divertor is taken into account.[30] Analysis of disruptions using the recently installed wide-angle infrared camera[31] provide qualitative data showing that a substantial amount of energy is deposited on the inner wall. Further analysis is required to identify the regions in which convected heat is deposited during disruptions.

III.C. Plasma Core Thermal Energy Losses Near and During JET Disruptions

The duration of the thermal quench obtained from the ECE electron temperature decay, together with the estimate of the plasma thermal energy approaching the disruption, has been used[26] to estimate the energy fluxes onto PFCs during the thermal quench. This estimate is naturally less accurate than the one obtainable using infrared data, but these are not easily available for disruptions. An estimate of the energy fluxes to PFCs in the predisruption stages is provided by evaluating the maximum derivative of the plasma thermal energy measured within 1 s of the thermal quench. To calculate the energy density reaching the PFCs, the corresponding wetted

area is necessary. Since this is generally not known, the wetted area during the performance deterioration has been taken to be equal to that of normal operation (1 m^2, in JET), while the largest possible broadening factor ($\sim$10) has been applied to the disruption power footprint. This broadening factor is based on measurements of the divertor power flux during disruptions in both ASDEX Upgrade[32] and JET (Ref. 33), which have shown that the divertor power deposition profile broadens by a factor of 5 to 10 during the disruption thermal quench with respect to the predisruption profile.

The estimated power densities under these assumptions are shown in Fig. 9a. The predisruptive PFC energy fluxes are comparatively small and do not exceed the estimated maximum divertor power fluxes of 130 MW/m^2 even in the discharges with the fastest performance deterioration in the last $\sim$1 s before the disruption. These are the only cases for which the predisruptive power fluxes can be expected to exceed the energy fluxes during the thermal quench itself. The estimated maximum divertor power fluxes during the thermal quench can be up to an order of magnitude larger (i.e., in the range of 1 GW/m^2). Indeed, for some of the discharges, the maximum divertor power flux can reach values of up to 2.3 GW/m^2 and systematically exceeds $\sim$0.5 GW/m^2 for the ITB disruptions caused by strong pressure peaking but remains under $\sim$0.5 GW/m^2 for other disruption types. The same data, expressed in terms of ϕ_{damage}, is plotted in Fig. 9b. The predisruptive ϕ_{damage} is smaller than 8 MJ m^{-2} $s^{-1/2}$. Although for non-ITB disruptions the thermal quench divertor load does not exceed 11 MJ m^{-2} $s^{-1/2}$, the ITB thermal quench ϕ_{damage} varies between 15 and 40 MJ m^{-2} $s^{-1/2}$. Since the wetted area used is based on the assumption of a tenfold broadening, ϕ_{damage} can reach up to 130 MJ m^{-2} $s^{-1/2}$ if the broadening is less than 3 (see error bars); this is sufficient to cause localized beryllium melting[34] ($\phi_{damage} \sim 16$ MJ m^{-2} $s^{-1/2}$), carbon ablation,[35] or tungsten melting (> 40 to 50 MJ m^{-2} $s^{-1/2}$).

On the basis of this analysis, the phase of the JET disruptions most likely to lead to a large energy flux onto the PFCs is the thermal quench, even though the plasma energy at this time is considerably lower than that of a full-performance plasma. The reasons for this are twofold: the relatively long timescales for predisruptive energy losses in our "high-energy" disruption database and the considerable difference in timescales between the current and thermal quench in JET (typically one order of magnitude or larger).

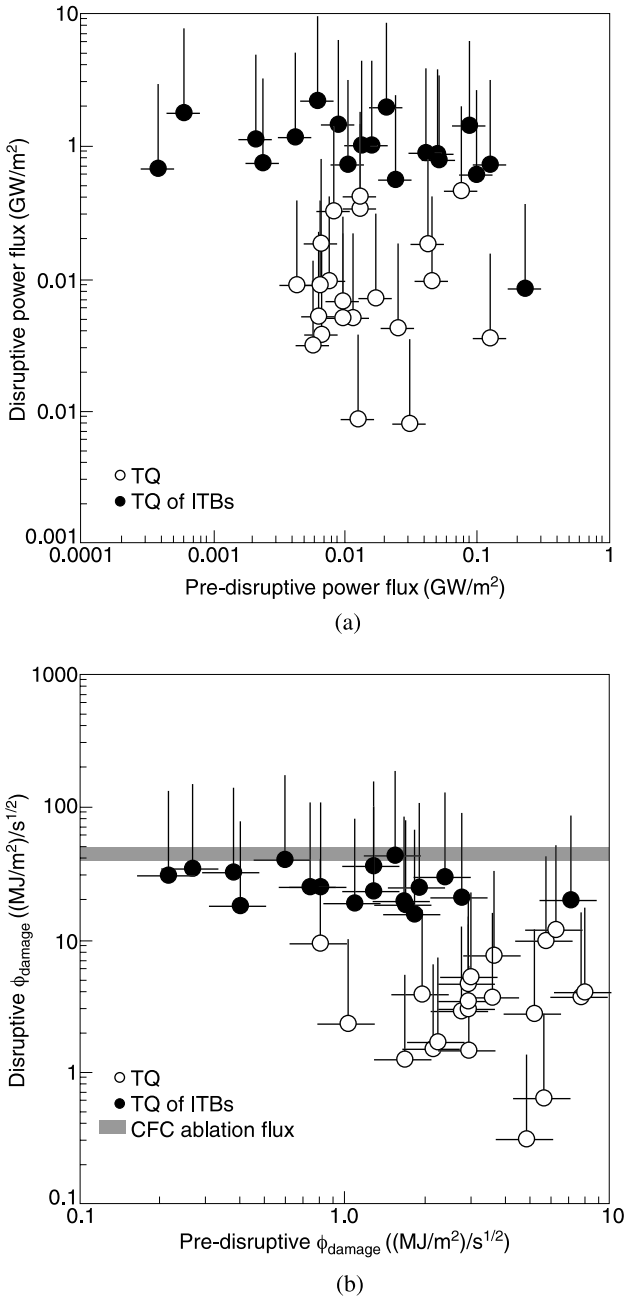

Fig. 9. Estimate of (a) the power density deposited on PFCs and (b) the "ablation/melting parameter" before (horizontal axis) and during (vertical axis, here also compared with the reference value for carbon fiber composite ablation and tungsten melting) the thermal quench for the "high-energy" disruption database in JET (Ref. 26).

III.D. Magnetic Energy Flow During Disruptions

During the plasma current decay, the energy stored in the poloidal magnetic field is dissipated, mostly by radiation due to ohmic heating of the cold resistive plasma. As the plasma current is inductively coupled to the vacuum vessel and poloidal field coils, magnetic energy may also be coupled to these. To estimate the amount of energy coupled out of the system, the self- and mutual inductances of all the conductors could be computed together with the full magnetic induction equation to determine the coupling.[22] Alternatively, the electromagnetic energy flux through a closed surface enclosing the plasma

can be measured, using Poynting's theorem.[30] The amount of energy coupled between the plasma and the external circuits has been calculated for 20 disruptions using Poynting's theorem; for two of these it has been compared to that previously estimated using the full induction equation method and shown to agree within 7%. The energy coupled with the external circuits has also been compared with the initial self-magnetic energy of the plasma. The result of a linear fit showed 61% of initial self-magnetic energy is coupled with the external circuits, while the rest is radiated.

IV. OBSERVATION OF RUNAWAY ELECTRONS

Runaway electrons with energies of several MeV have been observed during numerous disruptions in JET (Refs. 36 through 41) and other large tokamaks.[42–45] The interaction of the runaway electron beams with the PFCs resulted in large heat loads and melting, even of the vacuum chamber itself. In future reactor-scale devices, like ITER (Ref. 2), localized deposition of multi-MeV runaway electron beams on the first wall is likely to cause severe damage. A good understanding of the runaway electron phenomenology will improve the chances of coping with (or avoiding) runaway electrons in operation at high plasma current, where they are most dangerous and likely to occur.

In the original survey of JET shots with runaway electron production,[37] the variations in behavior caused by different configurations (including carbon and beryllium limiters) were identified and subsequently were analyzed.[36,38] After the installation of the divertor, rather few discharges had long-lasting runaway electrons, and this is attributed to the more vertically unstable plasma columns caused by the nonsymmetric configuration.[39] A recent examination of the hard X-ray emission following disruptions[41] showed that many discharges had some spontaneous runaways even though the characteristic plasma current plateau did not develop. Although the likelihood that the runaway electron beam lasts several milliseconds is higher for plasma disrupting at low elongation or with good vertical stability (i.e., those before the divertor was installed), no trend in runaway electron generation has been found with the elongation (an initial burst of runaway electrons can be observed at any elongation).

A survey of a large number of JET discharges shows that runaway electrons occur after a disruption when the value of the toroidal field exceeds the threshold of 2 T, similar to JT-60U (Ref. 42) and TORE-SUPRA (Ref. 45). In addition, the number of photo-neutrons [produced via (γ, n) interaction with the wall by colliding runaway electrons with energy higher than 10 MeV] increases by two orders of magnitude as the toroidal field goes from 2 to 3.5 T; a similar enhancement in the strength of the runaway electron population has been observed in FTU (Ref. 46). The JET data show no clear threshold on the value of the boundary safety factor, q_{95}. This is present in the JT-60U data,[42] however, in which no runaway electrons are observed for $q_{95} < 2.5$ at the disruption. Finally, the number of photo-neutrons has an upper limit, which scales with the initial plasma current decay rate.

SXR emission tomography reconstruction has been carried out for pulse 53 790, which was deliberately designed to produce and maintain runaway electrons.[47] Hard X-ray bursts during the negative loop voltage spikes show that a substantial runaway electron population, with energy in the MeV range, has been created in the early stages of the disruption and survived until the current quench phase. The analysis shows that confinement conditions for the existing population of superthermal or low-energy runaway electrons are created very soon after magnetic flux reconnection. As the runaway electrons gain more energy at the current quench, the SXR bursts become a consequence of the interaction of the runaway electron beam with the wall and bursts of hard X-rays and neutron emissions appear at the same time.

A very similar event, pulse 53 786, has been analyzed with a zero-dimensional model[40] and subsequently with the ARENA code,[4] which solves the relativistic drift kinetic equation for electrons in toroidal geometry. The ARENA codes takes into account both primary (Dreicer) and secondary (avalanche[48,49]) runaway production, so the evolution of the toroidal electric field is calculated self-consistently: The current carried by the runaways modifies the electric field responsible for the runaway production in the first place, making the dynamics nonlinear. There is good agreement between the computed electric field and the measured toroidal voltage and also between the computed and measured plasma current converted into runaway electron current. The ARENA code is also able to compute the runaway electrons' energy spectrum. In the case studied, it consisted of two parts: a drawn-out tail and a high-energy "bump." The bump is mainly made up of primary (Dreicer) runaway electrons, while the tail represents secondary (avalanche) electrons.

Runaway electron prevention was achieved by puffing He before slowly injecting a high-Z gas in outer limiter configuration. The injection of high-Z gas alone in this plasma configuration reliably leads to runaway electron generation (pulses 54 047 and 63 114 in Fig. 10), but preemptive helium injection (pulses 54 048 and 63 113 in Fig. 10) prevents runaway electron generation. There is no difference in runaway electron generation (or lack of generation) between the cases with [54 047-8 (Ref. 22)] and without (63 113-4) ion cyclotron resonance frequency power.

In JT-60U (Ref. 50), the presence and strength of runaway electron beams was shown to be dependent on the amplitude of the externally imposed error field. In JET it was already observed[40] that magnetic fluctuations prevent runaway electron generation at JET, but these were naturally occurring and not applied on purpose. Only recently, one set of the external field correction

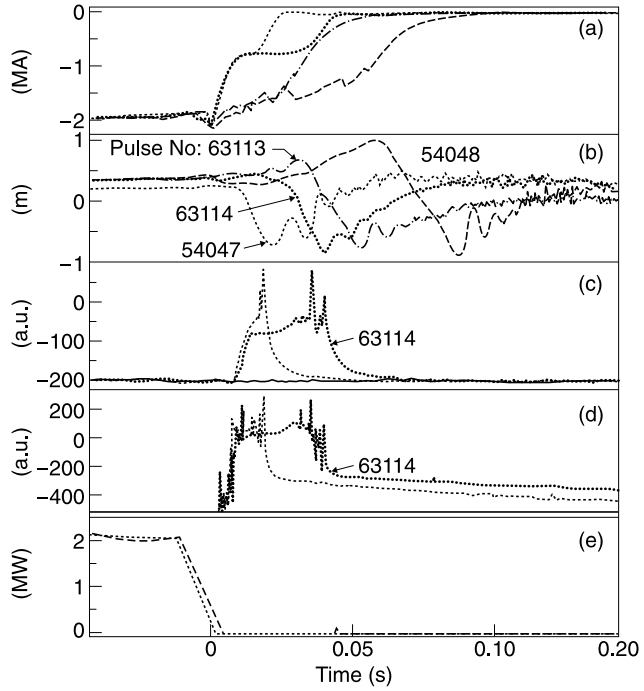

Fig. 10. (a) Plasma current, (b) vertical position, (c) hard X-ray, (d) photo-neutron emission, and (e) lower hybrid and ion cyclotron resonance heating (ICRH) power, in six runaway electron study discharges: 54048 with ICRH and He puff, 54047 with ICRH (reference), 63113 without ICRH and with He puff, and 63114 without ICRH (reference). All discharges have the time offset to the start of the thermal quench.

coils[51] (EFCCs) has been energized before the planned disruption of limiter plasmas. The toroidal field was varied between 2.6 and 2.3 T; all the plasma had the same disruption q, with the largest toroidal field discharge being run at 1.75 MA. The number of photo-neutrons decreases by two orders of magnitude when the EFCC is applied at 2.6 T. Photo-neutrons are observed in the 2.3-T case without EFCC, but they are below the resolution for the 2.3-T case with EFCC and for cases both with and without EFCC at 2.45 T.

V. DISRUPTION PREDICTION AND MITIGATION

Disruption prediction and mitigation will have to be an integral part of all plasma operations in ITER, in which heat loads, electromechanical loads, and runaway electrons must be controlled. This requirement poses stringent objectives to the present tokamaks in developing and evaluating, in operating conditions as relevant to ITER as possible, the necessary disruption prediction and mitigation techniques. JET can offer some of the most ITER-relevant operating conditions, but it was and still is insufficiently equipped to test mitigation techniques. On the other hand, in recent years an increasingly substantial effort has been spent in developing disruption detection tools.

V.A. Classification and Prediction of Disruptions Using Neural Networks

Since disruptions can occur in different regions of the operating space and, depending on the mode of operation, have different precursors, it is impossible to define a mathematical model predicting deterministically their onset. However, statistical data analysis and the experience gathered during several years of operation are used to train neural networks—systems able to estimate the probability of a disruption taking place within a time sufficient to carry out ameliorating actions.

Work on disruption prediction started in the 1990s at JET (Ref. 52). This work and similar work in other tokamaks[53–54] were then used as a basis for the development of a disruption classification tool,[55] and a prediction neural network, with the potential of becoming an on-line tool, has been developed.[56]

Statistical and neural pattern recognition techniques have been used to develop an automatic disruption classifier. The data used to train and test the classifiers belong to four disruption classes (mode lock, density limit/high radiated power, H-mode/L-mode transition, and ITB plasma disruptions), each described by a large number of diagnostic signals also available in real time. For a limited number of pulses, class membership has been obtained via manual classification, to ensure the correct design and/or validation of the classifier. Multilayer perceptron classifiers exhibited the best performance, which can be further improved using multiple classifiers. The simple average of the output of individual classifiers and majority voting with rejection options have been implemented. The classification tool finally implemented at JET combines the outputs of five multilayer perceptron classifiers.

The predictive system structure consists of a cascade of a clustering block, and a neural disruption predictor. The clustering procedure is carried out by a self-organizing map, with the key feature of having the output array nodes arranged such that neighboring nodes represent similar patterns and nodes that are well separated represent different patterns. The disruption predictor is a traditional multilayer perceptron, composed of layers of neurons in which the input layer is connected to the output layer through the hidden neurons. The training process is undertaken by changing the connection weights such that a desired input-output relationship is realized. The network has been trained in the flattop of X-point configuration with plasma current >1.5 MA. The training set used consists of 69 disrupted pulses, and the validation set consists of 17 disrupted pulses. The test set used consists of 86 disrupted pulses and 102 successful

TABLE II

Neural Network Performance Results

	Training Set	Validation Set	Test Set
Missed alarms	—	3/17 (17.6%)	28/86 (32.5%)
False alarms	3/69 (4.3%)	—	11/188 (5.8%)

pulses. Results with the best network configuration (composed of 9 inputs, 1 hidden layer with 15 hidden neurons, and 1 output, resulting in 166 network parameters) are summarized in Table II. Here, a false alarm is when two consecutive outputs above a preset threshold occur in a successfully terminated pulse or, in a disrupted pulse, occur more than 1 s before the disruption, and a missed alarm is when at least two consecutive outputs are not greater than a preset threshold in the last 100 ms before the disruption. The network performance is good in terms of false alarms, whereas it still presents a quite high percentage of missed alarms. This is because the configuration was optimized toward minimizing false alarms; a different optimization could reduce the number of missed alarms.

More recently attention has been focused on "novelty detection." When new plasma configurations present features significantly different from those observed in the experiments used during the training phase, the neural network is likely to fail (either cause a false alarm or spuriously terminate a discharge). To reduce such occurrences, a novelty detection method, which determines the novelty of the input of the prediction system, can be used to assess the network reliability. This is useful for JET, in which plasma configurations evolve rapidly as part of the exploratory nature of its operation, and in the long term for ITER, since it will minimize the amount of disruptions needed to train a reliable disruption detection network. Thus, novelty detection is one of the fundamental requirements of a good classification or prediction system. The tool developed for JET (Ref. 57) consists of two blocks mutually connected: a self-organizing map and a support vector machine predictor. During the training phase, the self-organizing map performs a clustering procedure and the support vector machine predictor is trained to give the alarm in case of impending disruption. When the training procedure is completed, bands that will enable the network to discriminate between novel and nonnovel samples are defined. When in use, samples that fall outside the nonnovel band are recognized, and if the corresponding alarm is triggered, this is ignored. This results in fewer false alarms but potentially in more missed alarms when working in new operation spaces.

V.B. Mitigation of Disruption by Gas Puffing

The aims of disruption mitigation are as follows:

1. to reduce the amount of energy conducted to the divertor
2. to reduce the electromechanical loads on the vessel and the in-vessel components
3. to avoid runaway electron generation.

So far JET has attempted only the reduction in electromechanical loads and partially the runaway electron avoidance (discussed in Sec. IV). These experiments were carried out using the two valves of the JET standard gas injection, which can operate at relatively high pressure, 2.5 bar. The maximum amount of injected impurity was 9×10^{21} atoms in <50 ms. Three gases have been employed (helium, neon, and argon), always in feed-forward injection (i.e., preprogrammed deliberate disruption, independent from any input from the plasma). In deliberate VDEs, the main effect of the helium injection was to slow down the disruption, leading to overall more demanding electromagnetic loads (e.g., vessel forces[22]). Instead, neon and argon were sufficient to transform a potential VDE into a density limit disruption and significantly reduce the electromechanical loads. With gas injection the vessel electromechanical loads and the halo current depend only on the delay between the thermal quench and the loss of vertical equilibrium position, as shown in Fig. 11. The current quench characteristics of the disruptions caused by Ar and Ne puffs are similar to these of density limit or radiative collapse disruptions (i.e., globally faster than in VDEs). Therefore, while the vessel electromechanical loads are reduced, those on the in-vessel component could be

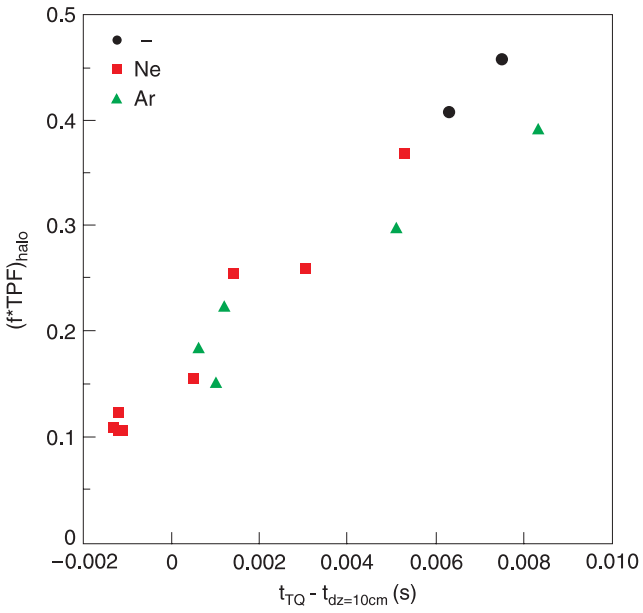

Fig. 11. Product of halo fraction and TPF as a function of the delay between thermal quench (due to gas puff where indicated in the legend) and loss of vertical stability; all discharges had the same plasma configuration and current.

increased, especially if high-conductivity material (e.g., Be in the near future for JET and in the long term for ITER) is used.

The limited scope of the JET investigation is due to several limitations:

1. The gas injection system was able to deal with only small quantities of gas at relatively low pressure; in consequence, the theory that runaway electron generation is stopped by the background electron density being high enough to bring the critical electrical field beyond what the current quench can induce could not be tested, and massive gas jets such as those used in DIII-D (Ref. 58), TEXTOR (Ref. 59), and ASDEX Upgrade[60] could not be achieved.

2. The diagnostic systems, in particular infrared thermography, cannot cope with disruptions (slow sampling rates, restricted views); in consequence, comparison between heat load without and with mitigation could not be carried out.

The first of these limitations has been addressed by installing (in early 2006) a new fast injection valve, similar to the one used in TEXTOR (Ref. 61), independent from the rest of the JET gas injection system. The main features of the new valve are rapid gas injection in the torus (2-ms opening time and ~15-ms delivery time at sound speed); a large amount of injected gas, potentially more than 10 bar ℓ (gas reservoir volume of 0.65 ℓ and operating pressure of up to 35 bar, with up to 50% of the reservoir emptied) corresponding to 2.7×10^{23} atoms; and the capability of working in a relatively high magnetic field. The new valve will be used to inject Ar at full performance and He at reduced pressure (to avoid spontaneous regeneration of the divertor and the neutral beam box cryopumps). The specifications of this valve make JET able to perform plasma terminations by massive gas jets and possibly allow runaway electron prevention, which requires a background electron density at least 100 times larger than the predisruption plasma density.

V.C Neutral Point

Large electromechanical loads can be avoided also by working at or close to the neutral point. This is the position at which the initial plasma vertical displacement δz_0 vanishes, or has a minimum, so the plasma vertical displacement, which can be written as $\delta z = \delta z_0 \exp[\gamma(t - t_0)]$ (where t_0 is the time when the perturbation is given and γ is the vertical instability growth rate) can be minimized.

A first set of experiments was performed using the radiative collapse of small plasmas, which could be set over a large range of vertical positions without changing shape (constant elongation and triangularities) or boundary safety factor, and hence vertical growth rate. The neutral point for that combination of configuration and disruption cause was found experimentally and confirmed analytically using the CREATE L code.[62]

A second set of experiments was aimed at studying the spatial dependence of the excitation of the unstable mode following an ELM (Ref. 63). The CREATE L linearized plasma response model was used to reliably estimate the growth rate and provide input to the correct global characterization of ELMs from the point of view of simplified modeling for control. The vertical growth rate was not constant in these discharges, because the plasma centroid had to move radially as well as vertically in order to keep the plasma-to–divertor coil current ratio compatible with neutral beam injection. In addition, the size of the ELM at which the vertical control system was switched off was not always the same, so neither was the perturbation magnitude. Once the vertical displacement measured after a certain amount of time was scaled to a reference growth rate and normalized with respect to the perturbation magnitude, it was found to be a linear function of the vertical position, with its zero just outside the vertical range explored during the experiment.

VI. CONCLUSIONS AND OUTLOOK

JET has significantly progressed in the characterization of disruptions and continues to contribute to the disruption databases.[64]

The sources of electromechanical loads during disruptions have been quantified. Vessel symmetric forces depend on the plasma current and configuration, as well as the type of disruption. Vessel asymmetric forces can be linked to the macroscopic asymmetry of the plasma, although the causes of this asymmetry have not been fully understood.

The energy loss from the plasma core at the thermal quench is relatively well understood. On the other hand, further work is necessary to quantify the PFC heat load at the thermal quench; both the temperature rise time and the footprint extent still need to be fully characterized in JET.

Thanks to the ability to work at relatively high plasma currents and to the machine size, JET is an ideal setup to study runaway electrons. Over the years JET has built up a substantial database on runaway electron generation (e.g., toroidal field threshold and survival, but not generation, depending on vertical stability). However, no detailed measurement of the energy spectrum is available, even if this is an important clue in understanding the experimental contribution of avalanche to the runaway electron population and therefore consolidate predictions for ITER disruptions.

Although disruption prediction and mitigation will be a key feature of the next-generation machines, progress in the investigation of gas injection–based disruption mitigation techniques in JET has been constrained due to

hardware limitations, which have now been addressed, and has suffered from the same diagnostics limitations as the study of disruption heat loads. On the other hand, in recent years JET disruption classification and prediction neural networks have been developed for JET. In addition, novelty detection techniques are being investigated to improve neural network performance.

ACKNOWLEDGMENTS

This work was partly funded jointly by the United Kingdom Engineering and Physical Sciences Research Council and by the European Communities under the contract of Association between EURATOM and UKAEA. The views and opinions expressed herein do not necessarily reflect those of the European Commission.

The author thanks all those who have contributed to the JET disruption studies presented in this paper, in particular P. Noll for mentoring on vertical displacement events and inspiring the analysis of asymmetric VDEs and P. Lomas and A. Loarte for the fruitful discussions on disruption-related machine integrity and disruption heat loads, respectively.

REFERENCES

1. J. WESSON, *Tokamaks*, Clarendon Press, Oxford (2004).

2. ITER PHYSICS EXPERT GROUP ON DISRUPTIONS et al., "ITER Physics Basis," *Nucl. Fusion*, **39**, Chap. 3, Sec. 4 (1999).

3. G. FEDERICI, *J. Nucl. Mater.*, **313–316**, 11 (2003).

4. L. G. ERIKSSON and P. HELANDER, *Comput. Phys. Commun.*, **154**, 175 (2003).

5. V. RICCARDO, *Fusion Sci. Technol.*, **43**, 493 (2003).

6. P. ANDREW et al., "The Relation Between Halo Currents and Plasma Displacement/Deformation in JET," *Proc. 17th SOFE*, San Diego, California (1997).

7. V. RICCARDO et al., *Fusion Eng. Des.*, **66–68 A**, 919 (2003).

8. V. RICCARDO et al., *Plasma Phys. Control. Fusion*, **46**, 925 (2004).

9. P. SONATO et al., *Fusion Eng. Des.*, **74**, 757 (2005).

10. V. RICCARDO, "Asymmetric Vertical Displacement Events in JET," PhD Thesis, Imperial College, London (1998).

11. M. SUGIHARA et al., "Analysis of Disruption Scenarios and Their Mitigation in ITER," *Proc. 20th IAEA Int. Conf. Fusion Energy*, Vilamoura, Portugal (2004).

12. V. RICCARDO et al., *Plasma Phys. Control. Fusion*, **47**, 117 (2005).

13. P. NOLL et al., *Fusion Technol.*, **15**, 259 (1989).

14. A. TANGA, "Disruptions and Vertical Displacement Events in JET," *Proc. 16th IAEA Int. Conf. Fusion Energy*, Montreal, Canada (1996).

15. V. RICCARDO et al., *Fusion Eng. Des.*, **47**, 389 (2000).

16. A. KAYE, "Sideways Displacements of the Torus," Annex 4 in the Joint JET-JSC-RAG Report to the 65th JET Scientific Council (Mar. 1997).

17. T. RAIMONDI, "Some Results from the Sideways Model," Annex 5 in the Joint JET-JSC-RAG Report to the 65th JET Scientific Council (Mar. 1997).

18. M. BUZIO, "Structural Effects of Plasma Instabilities on the JET Tokamak," PhD Thesis, Imperial College, London (1998).

19. V. RICCARDO et al., *Nucl. Fusion*, **40**, 1805 (2000).

20. T. EICH et al., "Analysis of Power Deposition in JET MKIIGB Divertor by IR-Thermography," *Proc. 28th EPS Conf. Plasma Phys.*, Madeira, Portugal (2001).

21. V. RICCARDO et al., *Plasma Phys. Control. Fusion*, **43**, 881 (2001).

22. V. RICCARDO et al., *Plasma Phys. Control. Fusion*, **44**, 905 (2002).

23. E. DE LA LUNA et al., *Rev. Sci. Instrum.*, **75**, 3831 (2004).

24. L. C. INGESSON et al., *Nucl. Fusion*, **38**, 1675 (1998).

25. J. P. CHRISTIANSEN et al., *J. Comput. Phys.*, **73**, 85 (1987).

26. V. RICCARDO and A. LOARTE, *Nucl. Fusion*, **45**, 1427 (2005).

27. G. FEDERICI et al., *Plasma Phys. Control. Fusion*, **45**, 1523 (2003).

28. G. FEDERICI et al., *J. Nucl. Mater.*, **313–316**, 11 (2003).

29. G. PAUTASSO et al., "Details of Power Deposition in the Thermal Quench of ASDEX Upgrade Disruptions," *Proc. 31st EPS Conf. Plasma Physics*, London, England (2004).

30. J. PALEY et al., *J. Nucl. Mater.*, **337–339**, 702 (2005).

31. P. ANDREW et al., "Main Chamber Power Load During Disruptions," *Proc. 17th Int. Conf. Plasma Surface Interactions in Fusion Devices*, Hefei Anhui, China (2006).

32. G. PAUTASSO et al., *Proc. 30th EPS Conf. Plasma Physics*, St. Petersburg, Russia (2003).

33. P. ANDREW et al., *Proc. 30th EPS Conf. Plasma Physics*, St. Petersburg, Russia (2003).

34. A. LOARTE et al., *J. Nucl. Mater.*, **337–339**, 816 (2005).

35. A. LOARTE, *Physica Scripta*, **T111**, 13 (2004).

36. J. WESSON, R. D. GILL, M. HUGON, et al., *Nucl. Fusion*, **29**, 641 (1989).

37. G. R. HARRIS, "Comparisons of the Current Decay During Carbon-Bounded and Beryllium-Bounded Disruptions in JET," JET-R(90)07 (1990).

38. R. D. GILL, *Nucl. Fusion*, **33**, 1613 (1993).

39. R. D. GILL et al., *Nucl. Fusion*, **40**, 163 (2000).

40. R. D. GILL et al., *Nucl. Fusion*, **42**, 1039 (2002).

41. V. RICCARDO, *Plasma Phys. Control. Fusion*, **45**, A269 (2003).

42. R. YOSHINO and S. TOKUDA, *Nucl. Fusion*, **40**, 1293 (2000).

43. Y. KAWANO et al., *Fusion Sci. Technol.*, **42**, 298 (2002).

44. E. D. FREDRICSON et al., *Phys. Plasmas*, **4**, 1589 (1997).

45. G. MARTIN, "Runaway Electrons: From TORE-SUPRA to ITER," *Proc. 25th EPS Conf. Plasma Physics*, Prague, Czech Republic (1998).

46. F. M. POLI, B. ESPOSITO, and G. MADDALUNO, "Disruption Generated Runaways in FTU High Field Tokamak," *Proc. 43rd APS Conf. Plasma Physics*, Long Beach, California (2001).

47. V. V. PLYUSNIN et al., *Nucl. Fusion*, **46**, 277 (2006).

48. M. N. ROSENBLUTH and S. V. PUTVINSKI, *Nucl. Fusion*, **37**, 1355 (1997).

49. P. HELANDER, L. G. ERIKSSON, and F. ANDERSSON, *Plasma Phys. Control. Fusion*, **44**, B247 (2002).

50. Y. KAWANO et al., "Fast Current Shutdown Scenario for Major Disruption Softening in JT-60U," *Proc. 16th IAEA Int. Conf. Fusion Energy*, Montreal, Canada (1996).

51. M. BIGI et al., *Fusion Eng. Des*., **58–59**, 189 (2001).

52. F. MILANI, "Disruption Prediction at JET," PhD Dissertation, University of Aston in Birmingham, England (1998).

53. G. PAUTASSO et al., *Nucl. Fusion*, **42**, 100 (2002).

54. R. YOSHINO, *Nucl. Fusion*, **43**, 1171 (2003).

55. B. CANNAS et al., *Nucl. Fusion*, **46**, 699 (2006).

56. B. CANNAS, "Neural Approaches to Disruption Prediction at JET," *Proc. 31st EPS Conf. Plasma Physics*, London, England (2004).

57. R. DELOGU, "Support Vector Machines for Disruption Prediction and Novelty Detection at JET," *Proc. 24th SOFT*, Warsaw, Poland (2006).

58. D. G. WHYTE, T. C. JERNIGAN, D. A. HUMPHREYS et al., *J. Nucl. Mater*., **313**, 1239 (2003).

59. K. H. FINKEN et al, *Nucl. Fusion*, **41**, 1651 (2001).

60. G. PAUTASSO and O. GRUBER, *Fusion Sci. Technol*., **44**, 716 (2003).

61. A. SAVTCHOV, K. H. FINKEN, and G. MANK, *Rev. Sci. Instrum*., **73**, 3490 (2002).

62. F. VILLONE et al., *Fusion Eng. Des*., **66–68**, 709 (2003).

63. F. VILLONE et al., *Nucl. Fusion*, **45**, 1328 (2005).

64. J. WESLEY et al., "Disruption Characterization and Database Activities for ITER," *Proc. 21st IAEA Int. Conf. Fusion Energy*, Chengdu, China (2006).